J. Phys.: Condens. Matter 5 (1993) 7771–7784. Printed in the UK

Computation of parametric x-ray production by relativistic particles in crystals under multiple Bragg diffraction

I Ya Dubovskaya, S A Stepanov, A Ya Silenko and A P Ulyanenkoff
Institute for Nuclear Problems, 11 Bobruiskaya Street, 220050 Minsk, Republic of Belarus

Received 20 April 1993

Abstract. An algorithm for computing spectral-angular and angular distributions of parametric x-ray radiation (PXR) produced by ultrarelativistic particles in crystals under multiple Bragg diffraction is developed. The algorithm is based on the methods applied in the dynamical theory of x-ray multiple diffraction. The angular distribution of three-wave PXR angular distribution into the simulated forbidden reflex (222) in the Ge crystal is computed. It is shown that using multiple PXR generation it is possible to generate x-ray beams with double angular collimation $\simeq$ 1 angular s^2 and spectral width $\simeq 10^{-3}$.

1. Introduction

Parametric (quasi-Cherenkov) x-ray radiation (PXR) is the radiation produced by a relativistic particle moving with a constant velocity through a crystal target. One of the main peculiarities of PXR is that the x-rays can be observed not only at a small angle along the particle movement but also at a large angle (the Bragg angle). The physical principle of PXR production is similar to that of Cherenkov emission in the optical band but it strongly requires periodic (crystalline) media. The fact is that the refractive index of x-rays in uniform media is known to be smaller than unity (the phase speed of x-rays is more than the light speed constant) and therefore x-ray Cherenkov radiation is impossible. However, under the Bragg condition for x-rays emitted in a crystal, the situation can change. Due to dynamical diffraction the refractive index of x-rays can stand out above unity and, as a result, the Cherenkov condition can be fulfilled. This mechanism of PXR production was first predicted in [1] and experimentally confirmed in [2, 3].

From the viewpoint of applied physics PXR can be considered as a tunable frequency source of quasi-monochromatic x-rays [4]. In this connection the production of PXR under multiple diffraction is of great interest as the multiwave Bragg geometry is assumed to provide an enhancement of PXR spectral-angular density [5]. Moreover, the measurements of PXR angular distributions under four- and eight-wave diffraction conditions were carried out in [7, 8]. In these experiments intensive narrow peaks resulting, as the authors supposed, from the multiwave diffraction, were observed.

Up to now the theoretical interpretation of PXR experiments was restricted to the case of two-wave diffraction when simple analytical expressions can be derived [8, 9]. The multiwave generation of PXR can only be calculated using computers and has not been carried out because the respective algorithm was not developed. One of the solutions of this problem was proposed in [10, 11] on the basis of matrix exponentials. However, we think that this approach is convenient only for analytical analysis of the main features of

0953-8984/93/417771+14$07.50

PXR and is not applicable to computations because of the need to compute exponents of complex matrices.

In this paper the algorithm of computer simulation of multiwave PXR spectral-angular and angular distributions is developed on the basis of methods applied in the dynamical theory of x-ray multiple diffraction [12, 13]. The result is illustrated with the computation of three-wave PXR angular distribution in the direction of the simulated forbidden reflex (222) in the Ge crystal.

As we will show below the algorithm is suitable for an arbitrary multiwave PXR production. Therefore, its application to simulation of experiments [6, 7] requires only an account of the specific experimental geometry and spreadings. A detailed analysis of these experiments will be made in a separate publication.

2. Computation of PXR spectral-angular density

Let a relativistic charged particle (for definiteness, an electron) be incident on a crystal at such an angle that pseudophotons of particle electromagnetic field with a frequency ω and wave vectors directed along the particle velocity $\boldsymbol{v}$ satisfy the Bragg diffraction condition for several crystallographic planes with reciprocal lattice vectors $\boldsymbol{h}, \boldsymbol{g}, \ldots$ (see figure 1(*a*)). To find the x-ray wave field produced by the particle we should determine the Green-function of the problem and calculate its convolution with a current density produced by the moving particle. As shown in [1], the Green function can be expanded into a series of solutions of the homogeneous x-ray diffraction problem in the crystal. The substitution of this expansion into the convolution integral allows us to obtain the following expression for a number of PXR quanta emitted by a particle, for example, in a reflex $\boldsymbol{h}$ (we assume $\hbar = c = 1$):

$$\mathrm{d}N_{k_h\omega} = \left(\frac{e\omega}{2\pi}\right)^2 \left| \int_0^{t_L} \mathrm{d}t \left[\boldsymbol{v} \cdot \boldsymbol{E}^{(-)^*}_{k_h}(\boldsymbol{r}, \omega)\right] \exp(\mathrm{i}\omega t) \right|^2 \mathrm{d}\omega\, \mathrm{d}\Omega \tag{1}$$

where the integration is carried out over time $t_L = L/(\boldsymbol{v} \cdot \boldsymbol{n})$ of particle travel through the crystal target, L is the target length, $\boldsymbol{n}$ is the unit vector normal to the crystal surface, $\boldsymbol{r} = \boldsymbol{v}t$ is the radius vector of the particle coordinate, $\boldsymbol{k}_h = \omega\boldsymbol{v} + \boldsymbol{h}$ is the wave vector of a photon diffracted by crystallographic planes of $\boldsymbol{h}$, $\omega = \mid \boldsymbol{k} \mid$, and $\mathrm{d}\omega$ and $\mathrm{d}\Omega$ are the spectral and angular intervals where x-rays are detected. The magnitude of $P_{k,\omega} = \mathrm{d}N_{k,\omega}/\mathrm{d}\omega\ \mathrm{d}\Omega$ is the density of a spectral-angular distribution. The field amplitude $\boldsymbol{E}^{(-)^*}_k(\boldsymbol{r}, \omega)$ is the $\boldsymbol{k}$th component of the Green-function expansion in the solutions of the homogeneous problem. For a crystal with a finite size this field has an asymptotic form of a sum of a plane wave and incoming spherical waves. Previously, it was shown (see, for example, [1]) that the solutions of $\boldsymbol{E}^{(-)}_k$ and $\boldsymbol{E}^{(+)}_k$ are connected by the following relationship:

$$\boldsymbol{E}^{(-)^*}_k = \boldsymbol{E}^{(+)}_{-k} \tag{2}$$

where $\boldsymbol{E}^{(+)}_k$ is the solution of the homogeneous diffraction problem describing the scattering of a plane wave by a crystal.

So, the calculation of the $\boldsymbol{E}^{(-)}_{k_h}$ field can be reduced to the problem of multiple diffraction of a plane x-ray wave being incident on a crystal from the point where the detector, which records PXR photons with the wave vector $\boldsymbol{k}_h$, is placed (see figure 1(*b*)).

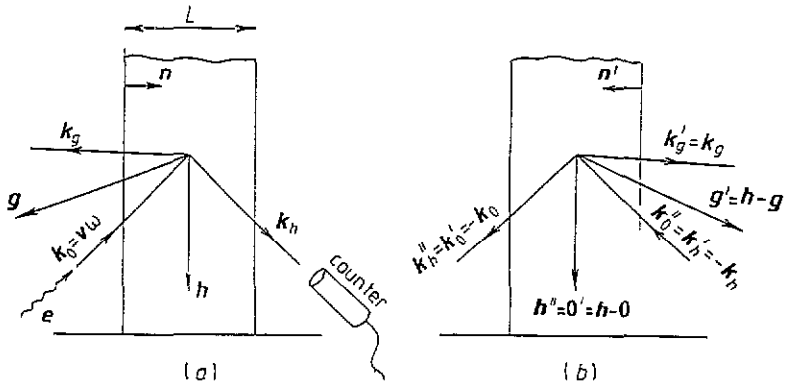

Figure 1. An illustration of the transition from the geometry of PXR emission (*a*) to the geometry of Bragg diffraction of an external wave propagating in the reversed direction (*b*).

Let us carry out the reversion of wave vectors in accordance with (2) and use the algorithm of the multiple Bragg diffraction problem, presented in [12] and [13]. The reversed wave vectors $\boldsymbol{k}'_m$ are introduced as $\boldsymbol{k}'_m = -\boldsymbol{k}_m$ ($\boldsymbol{m} = \boldsymbol{0}, \boldsymbol{h}, \boldsymbol{g}, \ldots$) and $\boldsymbol{k}'_h$ is assumed to be the wave vector of the incident wave. Then the reciprocal lattice vectors $\boldsymbol{m}'$ contained in the diffraction equation for the $\boldsymbol{k}'_h$ wave are connected with the initial vectors $\boldsymbol{m}$ by the relationship $\boldsymbol{m}' = \boldsymbol{h} - \boldsymbol{m}$. Really,

$$\boldsymbol{k}'_m = -\boldsymbol{k}_m = -(\boldsymbol{k}_0 + \boldsymbol{m}) = -(\boldsymbol{k}_h - \boldsymbol{h} + \boldsymbol{m}) = \boldsymbol{k}'_h + (\boldsymbol{h} - \boldsymbol{m}) = \boldsymbol{k}'_h + \boldsymbol{m}'.$$

Also, let $\boldsymbol{n}'$ be the crystal surface normal introduced at the surface of $\boldsymbol{k}'_h$ incidence in the way adopted in the diffraction problem. Obviously, $\boldsymbol{n}' = -\boldsymbol{n}$ for the Laue case and $\boldsymbol{n}' = \boldsymbol{n}$ for the Bragg one, i.e. $\boldsymbol{n}' = -(\gamma_h / \mid \gamma_h \mid)\boldsymbol{n}$ (γ_m are the cosines of the angles between the x-ray wave vectors and $\boldsymbol{n}$). As will be shown below, only two waves determine the PXR production: one that penetrates along the particle movement direction $\boldsymbol{k}'_0$ ($\boldsymbol{0}' = \boldsymbol{h}$) and one that is 'incident' from the registration point $\boldsymbol{k}'_h$ ($\boldsymbol{h}' = \boldsymbol{0}$). That is why it is convenient to denote the corresponding vectors in the following way: $\boldsymbol{k}''_0 = \boldsymbol{k}'_h$, $\boldsymbol{0}'' = \boldsymbol{0}$ and $\boldsymbol{k}''_h = \boldsymbol{k}'_0$, $\boldsymbol{h}'' = \boldsymbol{h}$; the primes will be omitted below.

Under the multiple Bragg diffraction the x-ray wave field $\boldsymbol{E}^{(+)}_{-k}(\boldsymbol{r}, \omega)$ can be represented inside a crystal as a sum of transverse Bloch waves of σ and π polarizations, which travel in all diffraction directions $\boldsymbol{k}_m$ and correspond to $2N$ dispersion branches [13] (N is the order of multiple diffraction):

$$\boldsymbol{E}^{(+)}_{-k}(\boldsymbol{r}, \omega) = \sum_{s=\sigma,\pi} \sum_{m} \boldsymbol{e}^s_m \cdot \mathcal{D}^s_m(\boldsymbol{r}) \tag{3}$$

$$\mathcal{D}^s_m(\boldsymbol{r}) = \sum_{j=1}^{2N} \lambda^{(j)} D^{s(j)}_m \exp\left\{i\left[\boldsymbol{k}_m - \omega(\epsilon^{(j)} - \alpha_m)\boldsymbol{n}\right]\boldsymbol{r}\right\} \tag{4}$$

where $\boldsymbol{e}^s_m$ are the unit vectors of σ and π polarizations ($\boldsymbol{e}^\sigma_m \perp \boldsymbol{k}_m$, $\boldsymbol{e}^\pi_m \perp \boldsymbol{k}_m$, $\boldsymbol{e}^\sigma_m \perp \boldsymbol{e}^\pi_m$). One has some freedom in choosing the directions of these vectors. We use the way adopted in [12] and [13], which is convenient for the case when all the reciprocal lattice vectors $\boldsymbol{h}, \boldsymbol{g}, \ldots$ are in the same plane. This is:

$$\boldsymbol{e}^\sigma_m = [\boldsymbol{s}_m \times \boldsymbol{h}_n] / \mid [\boldsymbol{s}_m \times \boldsymbol{h}_n] \mid \qquad \boldsymbol{e}^\pi_m = [\boldsymbol{e}^\sigma_m \times \boldsymbol{s}_m]$$

where $\boldsymbol{h}_n = [\boldsymbol{h} \times \boldsymbol{g}]$ is the normal to the plane and $\boldsymbol{s}_m = \boldsymbol{k}_m/\omega$ are the unit vectors along $\boldsymbol{k}_m$.

Parameters $\lambda^{(j)}$ are the coefficients of dispersion branches excitation which can be determined from the boundary conditions (see below); $D_m^{s(j)}$ are the field amplitudes for each branch. The parameters

$$\alpha_m = \left[(k_0 + m)^2 - \omega^2\right]/2\omega^2\gamma_m \qquad m = 0, h, g, \ldots \tag{5}$$

determine the deviation of an incident wave from the exact Bragg condition for the respective reflex. It should be noted that our definition of α_m differs by $1/2\gamma_m$ from that commonly used ($\gamma_m = (\boldsymbol{s}_m \cdot \boldsymbol{n})$). This definition was adopted to make the formulae more compact.

The parameters $\epsilon^{(j)}$ determine x-ray refraction at the crystal boundary as a function of α_m :

$$\boldsymbol{k}_m^{(j)} = \boldsymbol{k}_m - \omega(\epsilon^{(j)} - \alpha_m)\boldsymbol{n}. \tag{6}$$

The above relation results from the conservation of x-ray frequency under Bragg diffraction, the preservation of $\boldsymbol{k}_m$ tangential components at surface refraction and the fulfillment of the condition $\boldsymbol{k}_m^{(j)} = \boldsymbol{k}_0^{(j)} + \boldsymbol{m}$ for the Bloch waves in the crystal.

The wave amplitudes $D_m^{s(j)}$ and the parameters $\epsilon^{(j)}$ are sought as eigenvectors and eigenvalues of the dynamical diffraction equations in the crystal, which have the form [12,13]†:

$$\sum_{s'=\sigma,\pi} \sum_{m'} G_{mm'}^{ss'} D_{m'}^{s'(j)} = \epsilon^{(j)} D_m^{s(j)}. \tag{7}$$

Here

$$G_{mm'}^{ss'} = \alpha_m \delta_{mm'}^{ss'} - (1/2\gamma_m)\left\{\chi_{mm'}(e_m^s \cdot e_{m'}^{s'}) + \mathrm{i}\chi_{mm'}^{Q}\left[(s_m \cdot s_{m'})(e_m^s \cdot e_{m'}^{s'}) + (e_m^s \cdot s_{m'})(s_m \cdot e_{m'}^{s'})\right]\right\} \tag{8}$$

is the $2N \times 2N$ scattering matrix, $\chi_{mm'}$ and $\chi_{mm'}^{Q}$ are the dipole and quadrupole components of the expansion of the crystal dielectric susceptibility $\chi(\boldsymbol{r}, \omega)$ in a Fourier series over the reciprocal lattice vectors. To compute $\chi_{mm'}$ and $\chi_{mm'}^{Q}$ for an arbitrary x-ray frequency we used the program described in [14].

The set (7) is simply solved with a computer because the methods of numerical analysis of the eigenproblem are well developed, including the case of an arbitrary complex matrix. We used the reliable routine from [15] which was based on the reduction of the matrix to upper Hessenberg form and the LR algorithm.

To find the coefficients $\lambda^{(j)}$ one has to employ the boundary conditions for the wave amplitudes. For the plate-shaped crystal the conditions are

$$\mathcal{D}_m^{s(L)}(0) = \delta_{m0}[\delta^{s\sigma}\cos(\varphi) + \delta^{s\pi}\sin(\varphi)] \tag{9}$$

† Equations (7) are not valid one or more of the x-ray beams makes a grazing angle with the surface less than the critical angle of total external reflection ($\simeq 0.1$–1°). The two-beam grazing case has been considered in [17] and we plan to analyse a multiple-beam one in our next work.

for the Laue-case waves ($\gamma_m > 0$), and

$$\mathcal{D}_m^{s(B)}(L) = 0 \tag{9a}$$

for the Bragg-case waves ($\gamma_m < 0$).

Here δ_{m0} is the Kroneker symbol; φ designates the angular deviation of the 'incident' polarization from e_0^σ. Equations (9) with regard to (4) may be rewritten in the matrix form

$$\sum_{j=1}^{2N} C_m^{s(j)} \lambda^{(j)} = \delta_{m0}[\delta^{s\sigma} \cos(\varphi) + \delta^{s\pi} \sin(\varphi)] \tag{10}$$

where the following matrix has been introduced:

$$C_m^{s(j)} = \begin{cases} D_m^{s(j)} & \text{for } \gamma_m > 0 \\ D_m^{s(j)} \exp(-i\omega\epsilon^{(j)} L) & \text{for } \gamma_m < 0 \end{cases}. \tag{11}$$

The set of linear equations (10) is solved with respect to $\lambda^{(j)}$ by the Gaussian method using a computer. For this purpose an appropriate routine from [15] was applied.

Some remarks are in order here.

(1) As the particle produces x-ray photons with all polarizations simultaneously, one has to summarize the intensities over polarizations. The procedure includes the solution of (10) for the two right-hand terms; one is for σ-polarized 'incident' rays ($\varphi = 0$) and the other for π-polarized rays ($\varphi = 90°$). Then the obtained coefficients $\lambda_\sigma^{(j)}$ and $\lambda_\pi^{(j)}$ are used separately for computation of PXR intensities and the results are combined.

(2) If the crystal is thick (compared with x-ray absorption) the solutions of (7) with Im $\epsilon^{(j)} > 0$ should not be taken into consideration as they describe the waves reflected from the far boundary of the crystal plate. In this case the boundary conditions (9a) are not accounted for either and the total number of equations in (10) is reduced. The reader can find a detailed description of this reduction in [13].

Incidentally, we have found the wave fields inside the crystal as the solutions of (7) and (10). Substituting them in (1) and taking into account (2)–(4) we obtain

$$P_{k_h\omega} = \left(\frac{e\omega}{2\pi}\right)^2 \sum_{p=\sigma,\pi} \left| \sum_m \sum_{s=\sigma,\pi} \sum_{j=1}^{2N} (v \cdot e_m^s) \lambda_p^{(j)} D_m^{s(j)} \times \int_0^{t_L} dt \exp[i(k'_m r' + \omega t) - i\omega(\epsilon^{(j)} - \alpha_m)(n' \cdot r')] \right|^2 \tag{12}$$

where the sum over p denotes the summation over 'incident-wave' polarizations.

Let us express the coordinate vector in (12) in terms of time. In this case we have to account for the fact that in the Bragg case the coordinate origins of the diffraction and emission problems coincide and in the Laue case are misplaced by vt_L: $r = r' + vt_L$. Therefore

$$r'(t) = \begin{cases} v(t - t_L) & \text{for emission in the Laue-case reflex } (\gamma_h > 0) \\ vt & \text{for emission in the Bragg-case reflex } (\gamma_h < 0). \end{cases} \tag{13}$$

We should also note that the term $\boldsymbol{m} = \boldsymbol{h}$ in the summation over $\boldsymbol{m}$ is much greater than the others because the index of its exponent is small and can be equal to zero (neglecting absorption). Thereby, this term can give rise to strong Cherenkov emission. Neglecting the other terms corresponding to waves propagating under large angles to $\boldsymbol{v}$ and carrying out the integration in (12) taking account of the relation $t_L = L/\mid \gamma_h'' \mid$ and equation (13) we obtain

$$P_{k_h\omega} = \left(\frac{e\omega}{2\pi}\right)^2 \sum_{p=\sigma,\pi} \left| \sum_{s=\sigma,\pi} \sum_{j=1}^{2N} (\boldsymbol{v}\cdot\boldsymbol{e}_h^s)\lambda_p^{(j)} D_h^{s(j)} \left[1 - \exp(-\mathrm{i}Q^{(j)}L/\gamma_h)\right]/Q^{(j)} \right|^2 \tag{14}$$

where the following designation is used:

$$Q^{(j)} = (\boldsymbol{k}_h \cdot \boldsymbol{v} + \omega) + \gamma_h\omega(\epsilon^{(j)} - \alpha_h). \tag{15}$$

For a thick crystal equation (14) may be simplified:

$$P_{k_h\omega} = \left(\frac{e\omega}{2\pi}\right)^2 \sum_{p=\sigma,\pi} \left| \sum_{s=\sigma,\pi} \sum_{j=1}^{2N} (\boldsymbol{v}\cdot\boldsymbol{e}_h^s)\lambda_p^{(j)} D_h^{s(j)}/Q^{(j)} \right|^2. \tag{16}$$

Equations (14)–(16) provide the computation of the spectral-angular PXR distribution for an arbitrary number of Bragg reflexes involved, i.e. they solve the problem.

Concluding, the proposed simulation algorithm of multiwave PXR production consists of the following phases:

(1) evaluation of $\boldsymbol{v}$ and all $\boldsymbol{k}_m$ on the basis of the given reciprocal lattice vectors $\boldsymbol{m}$ and the frequency ω of PXR production;

(2) selection of the reflex $\boldsymbol{h}$ for which PXR production will be computed;

(3) evaluation of the vectors $\boldsymbol{k}_m'$, $\boldsymbol{h}_m'$ and $\boldsymbol{e}_m^s$ of the reversed diffraction problem and transition to the diffraction problem notations;

(4) computation of the crystal susceptibilities $\chi_{mm'}$ and $\chi_{mm'}^{Q}$;

(5) filling up the scattering matrix $G_{mm'}^{ss'}$ using equations (8) for given α_m;

(6) solution of eigenproblem (7) and evaluation of $\epsilon^{(j)}$ and $D_m^{s(j)}$;

(7) filling up the boundary condition matrix $C_{mm'}^{ss'}$ in accordance with (11);

(8) solution of the boundary problem (10) and evaluation of $\lambda_\sigma^{(j)}$ and $\lambda_\pi^{(j)}$ for the two 'incident' polarizations;

(9) evaluation of $Q^{(j)}$ using equation (15); and

(10) computation of PXR spectral-angular density by (14) or (16).

3. Construction of spectral-angular PXR distributions

If we intend to study $P_{k,\omega}$ depending on variations of ω and the diffraction angles we need to:

(i) determine how $\boldsymbol{k}_0$, $\boldsymbol{k}_h$ and $\boldsymbol{v}$ depend on the angles and $\delta\omega/\omega$;

(ii) use the dependences in the evaluation of α_m, $Q^{(j)}$ and $(\boldsymbol{v}\cdot\boldsymbol{e}_h^s)$; and

(iii) substitute the obtained α_m and $Q^{(j)}$ into (8) and (14).

Starting the analysis one reveals that, in two-wave PXR production, an arbitrary direction of particle motion through a crystal is a Bragg one. In fact, as the particle simultaneously emits x-rays with all frequencies, one can always match the Bragg condition ($\alpha = 0$) with some frequency. The situation is quite analogous to that of irradiation of the crystal by a collimated 'white' x-ray beam. From the Bragg condition for an x-ray quantum emitted along $\boldsymbol{v}$ ($\boldsymbol{k}_0^{\mathrm{B}} = \omega_{\mathrm{B}}\hat{\boldsymbol{v}}$) one can find (see (16)) that

$$(\omega_{\mathrm{B}}\hat{\boldsymbol{v}} + \boldsymbol{h})^2 - \omega_{\mathrm{B}}^2\hat{\boldsymbol{v}}^2 = 0 \tag{17}$$

and therefore

$$\omega_{\mathrm{B}} = -h^2/2(\hat{\boldsymbol{v}} \cdot \boldsymbol{h}) \tag{18}$$

where $\hat{\boldsymbol{v}} = \boldsymbol{v}/v = \boldsymbol{v}(1 + \frac{1}{2}\gamma^{-2})$ is a unit vector along $\boldsymbol{v}$; $\gamma = E/m$ is the gamma factor of the relativistic particle with energy E.

In the multiple-diffraction case the situation is not so arbitrary because the vector $\omega_{\mathrm{B}}\hat{\boldsymbol{v}}$ must fit at least two conditions like (17). Therefore, it must have an origin on the normal $\boldsymbol{h}_{\mathrm{n}}$ to the plane built by vectors $\boldsymbol{h}$, $\boldsymbol{g}$, ... (see figure 2). Tilts of $\boldsymbol{v}$ in the plane defined by $\boldsymbol{v}_{\mathrm{B}}$ and $\boldsymbol{h}_{\mathrm{n}}$ cause the movement of the origin along $\boldsymbol{h}_{\mathrm{n}}$ and thereby the variation of ω_{B} (the variation of the Ewald sphere radius). The conditions of multiple Bragg diffraction are preserved in this case. Otherwise, the tilts in the perpendicular direction (along $\boldsymbol{q}_v \equiv [\boldsymbol{v}_{\mathrm{B}} \times \boldsymbol{h}_{\mathrm{n}}]/\,|\,[\boldsymbol{v}_{\mathrm{B}} \times \boldsymbol{h}_{\mathrm{n}}]\,|$) cannot be compensated and give rise to deviations from the exact multiple Bragg diffraction condition†. Therefore, the vector $\boldsymbol{v}$ may be represented in the following form:

$$\boldsymbol{v} = \boldsymbol{v}_{\mathrm{B}}\left(1 - \tfrac{1}{2}\theta_v^2\right) + \theta_v\boldsymbol{q}_v = \hat{\boldsymbol{v}}_{\mathrm{B}} - \hat{\boldsymbol{v}}_{\mathrm{B}}\left(\tfrac{1}{2}\gamma^{-2} + \tfrac{1}{2}\theta_v^2\right) + \boldsymbol{Q}_v \tag{19}$$

where θ_v is the small angle between particle velocity and $\boldsymbol{v}_{\mathrm{B}}$. The latter is supposed to fit the multiple Bragg condition

$$(\omega_{\mathrm{B}}\hat{\boldsymbol{v}}_{\mathrm{B}} + \boldsymbol{m})^2 - \omega_{\mathrm{B}}^2 = 0 \qquad \boldsymbol{m} = \boldsymbol{h}, \boldsymbol{g}, \ldots. \tag{20}$$

To determine the variations of $\boldsymbol{k}_0$ one has to recollect that it was introduced as the 'incident' wave vector of the diffraction problem, being antiparallel to the momentum of x-ray photons generated in the direction of PXR registration. Therefore, this wave vector may be represented in the form

$$\begin{aligned}\boldsymbol{k}_0 &= \boldsymbol{k}_0^{(\mathrm{B})}\left(1 - \tfrac{1}{2}\theta_1^2 - \tfrac{1}{2}\theta_2^2\right) + \boldsymbol{k}_0^{(\mathrm{B})}\delta\omega/\omega + \omega_{\mathrm{B}}\left(\theta_1\boldsymbol{q}_1 + \theta_2\boldsymbol{q}_2\right) \\ &= \boldsymbol{k}_0^{(\mathrm{B})} + \boldsymbol{k}_0^{(\mathrm{B})}\left[\delta\omega/\omega - \tfrac{1}{2}\left(\theta_1^2 + \theta_2^2\right)\right] + \omega_{\mathrm{B}}\boldsymbol{Q}\end{aligned} \tag{21}$$

where

$$\boldsymbol{k}_0^{(\mathrm{B})} = -(\omega_{\mathrm{B}}\hat{\boldsymbol{v}}_{\mathrm{B}} + \boldsymbol{h}) \tag{22}$$

† Note that if vectors $\boldsymbol{h}$, $\boldsymbol{g}$, $\boldsymbol{t}$, ... do not lie in a common plane (as in [6] and [7]) then $\omega_{\mathrm{B}}\hat{\boldsymbol{v}}$ must have its origin at the crossing point of several $\boldsymbol{h}_{\mathrm{n}}$. In this case the direction of particle incidence into the crystal and the Bragg frequency are fixed.

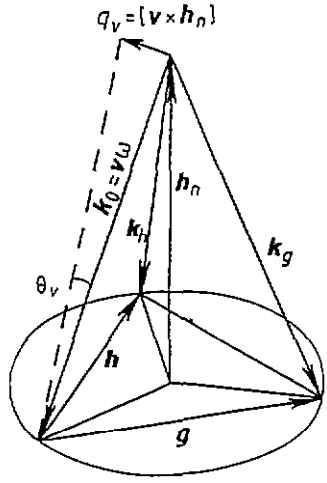

Figure 2. Geometry of non-coplanar three-wave diffraction of an x-ray photon emitted by a particle with velocity v.

is the wave vector matching the exact Bragg condition of the diffraction problem. In fact, with regard to (20) and the connection $m' = h - m$ one can find that

$$(k_0^{(B)} + m')^2 - k_0^{(B)} = 0 \qquad m' = h',\ g',\ \ldots. \tag{23}$$

The angles θ_1 and θ_2 introduced in (21) determine the angular deviations of k_0 from the exact Bragg condition. The term in (21) containing $\delta\omega/\omega$ characterizes the variation of length of k_0 due to variations of x-ray frequency. The vectors q_1 and q_2 are the unit vectors in the directions of θ_1 and θ_2 taking $q_1 \perp k_0^{(B)}$, $q_2 \perp k_0^{(B)}$, $q_1 \perp q_2$. The choice of the directions is usually given by directions in which the experimental angles are measured. More frequently used variants are

(a) $q_1 \parallel e_0^{\sigma}$ $\qquad q_2 \parallel e_0^{\pi}$

(b) $q_1 \simeq [h \times k_0^{(B)}]$ $\qquad q_2 \simeq [q_1 \times k_0^{(B)}]$.

We use (a).

To obtain the equation for k_h one can make use of the following relation which is easy derived from (6):

$$k_h = k_0 + h - \omega_B \alpha_h n. \tag{24}$$

Substituting (21) and (22) into (24) we obtain

$$k_h = -\hat{v}_B \omega_B + k_0^{(B)}\left[\delta\omega/\omega - \tfrac{1}{2}(\theta_1^2 + \theta_2^2) + \omega_B Q - \omega_B \alpha_h n. \right. \tag{25}$$

Finally, substituting (19), (21) and (25) into (5) and (15), we arrive at

$$\alpha_m = \omega_B^{-2}\gamma_m^{-1}\left\{(\boldsymbol{k}_0^{(B)}\cdot\boldsymbol{m})\left(\delta\omega/\omega - \tfrac{1}{2}(\theta_1^2+\theta_2^2) + \omega_B(\boldsymbol{Q}\cdot\boldsymbol{m})\right\}\right. \tag{26}$$

$$Q^{(j)} = \omega_B\left\{\tfrac{1}{2}(\gamma^{-2}+\theta_1^2+\theta_2^2+\theta_v^2) + \gamma_h(\epsilon^{(j)}-\alpha_h) - \boldsymbol{Q}_v\left[n\alpha_h + (h/\omega_B)\delta\omega/\omega - \boldsymbol{Q}\right]\right\}. \tag{27}$$

We would like to pay attention to a weak (square-law) dependence of $Q^{(j)}$ on angle $\boldsymbol{Q}_v$, i.e. deviation of a relativistic particle incidence direction from the multiwave condition. This provides good possibilities of observing multiwave PXR production in experiments because the averaging over $\boldsymbol{Q}_v$ due to a particle multiple scattering by a crystal will not have a strong effect.

Let us average equation (27) over the spread of the angle $\boldsymbol{Q}_v$. If the primary deviation of the particle velocity from the exact Bragg condition is not too large then the second bracket in (27) can be dropped and we can replace θ_v^2 by $\theta_v^2+\theta_s^2$ in the first bracket (see [1]). Here θ_s^2 is the mean square angle of multiple scattering given by the formula $\theta_s^2 = (E_s/E)^2(L/L_R)$; $E_s = 21$ MeV; L_R is the radiation length for the crystal. Thus, carrying out the averaging we obtain

$$Q^{(j)} = \omega_B\gamma_h\left(\Phi^2 + \epsilon^{(j)} - \alpha_h\right) \tag{28}$$

where $\Phi^2 = (\gamma^{-2}+\theta_1^2+\theta_2^2+\theta_v^2+\theta_s^2)/2\gamma_h$. Finally, applying (19) and (25) and the definitions of e_h^s and q_v one may obtain the expression for $(\boldsymbol{v}\cdot\boldsymbol{e}_h^s)$ in the linear approximation with respect to angles:

$$(\boldsymbol{v}\cdot\boldsymbol{e}_h^s) = (\boldsymbol{e}_h^{s(B)}\cdot\Delta\boldsymbol{s}_h) - \theta_v\delta^{s\sigma} \tag{29}$$

where $\delta^{s\sigma}$ is the Kroneker symbol; $\Delta\boldsymbol{s}_h = (\boldsymbol{k}_h - \boldsymbol{k}_h^{(B)})/\omega_B = \boldsymbol{Q} + \boldsymbol{k}_0^{(B)}\delta\omega/\omega^2 - \alpha_h\boldsymbol{n}$.

Equations (26)–(29) give the possibility of investigating the dependences of the spectral-angular density of PXR on θ_1, θ_2 and $\delta\omega/\omega$. Examples will be presented in section 6.

4. Computation of angular distributions

To compute the PXR angular distributions one has to integrate (14) and (16) over all possible deviations of PXR frequencies from the Bragg one ω_B †:

$$dN_{k_h} = \left(\frac{e\omega}{2\pi}\right)^2 \sum_{p=\sigma,\pi}\int_{-\infty}^{\infty}\left|\sum_{s=\sigma,\pi}\sum_{j=1}^{2N}(\boldsymbol{v}\cdot\boldsymbol{e}_h^s)\lambda_p^{(j)}(\omega)D_h^{s(j)}(\omega)/Q^{(j)}(\omega)\right|^2 d\left(\frac{\delta\omega}{\omega}\right). \tag{30}$$

In principle, the integration of (16) can be carried out numerically. However, the conventional algorithms will not work because the integrand function consists of a set of very narrow parametric resonance peaks, satisfying the condition

$$\mathrm{Re}\, Q^{(j)} = 0. \tag{31}$$

† It is also necessary to summarize over high-order Bragg frequencies $2\omega_B$, $3\omega_B$ ..., because the waves with vectors $2\boldsymbol{k}$, $3\boldsymbol{k}$, ... also undergo multiple diffraction on reciprocal lattice vectors $2\boldsymbol{m}$, $3\boldsymbol{m}$, ... We leave out this summation in assumption that the x-ray detector allows us to cut off the high-order frequencies.

The peak width with respect to $\delta\omega/\omega$ is of the order of $\operatorname{Im} Q^{(j)} \simeq \operatorname{Im}\epsilon^{(j)} \simeq \operatorname{Im}\chi_h$, while the integration band is $\simeq 10 \mid \chi_h \mid$, i.e. 10^3–10^4 times greater. Therefore, we have to find the frequency coordinates of PXR resonance peaks. From (31) and (28) we obtain

$$\operatorname{Re}\epsilon = \alpha_h - \Phi^2. \tag{32}$$

Substituting (32) in (7) we arrive at the equation set for the resonance frequencies:

$$\operatorname{Re}(G)\boldsymbol{D} = \operatorname{Re}(\epsilon)\boldsymbol{D} = (\alpha_h - \Phi^2)\boldsymbol{D}. \tag{33}$$

The unknown value $\delta\omega/\omega$ is presented in these equations through α_m, which, in accordance with (26), are linear in $\delta\omega/\omega$. A weak dependence $\chi_{mm'}(\omega)$ can be neglected. In principle, the solution of (33) is reduced to searching for the roots of a polynomial of rank $2N-2$, where N is the diffraction order. It is, however, known that the numerical root search of high-order polynomials is a very unstable procedure. Therefore, it is important to find a more effective algorithm. Equation (33) with regard to (8) and (26) can be transformed to the following form:

$$\mathbf{A}\cdot\boldsymbol{D} = (\delta\omega/\omega)\mathbf{B}\cdot\boldsymbol{D} \tag{34}$$

where $\mathbf{A}$ and $\mathbf{B}$ are square matrices:

$$A^{ss'}_{mm'} = \left(\alpha^{(0)}_m - \alpha^{(0)}_h + \Phi^2\right)\delta^{ss'}_{mm'} - \chi^r_{mm'}(e^s_m \cdot e^{s'}_{m'})/2\gamma_m \tag{35}$$

$$B^{ss'}_{mm'} = (f^\omega_h - f^\omega_m)\delta^{ss'}_{mm'} \tag{36}$$

$$\alpha^{(0)}_m = \alpha_m \mid_{\delta\omega/\omega=0} \qquad \chi^r_{mm'} = \operatorname{Re}\chi_{mm'} \qquad f^\omega_m = \omega_B^{-2}\gamma_m^{-1}(k_0^{(B)}\cdot m).$$

Equation (34) has the form of the generalized eigenvalue problem and we can apply for its numerical solution the algorithm described in [16] and realized in [15]. As the maximum power of $\delta\omega/\omega$ in this equation is $2N-2$, we shall obtain $2N-2$ roots and the same number of PXR peaks. However, some roots can be complex †. We take these roots into consideration too if their imaginary part is of the same order or less than the real one. In the case of complex roots the integration is carried out round $\operatorname{Re}(\delta\omega/\omega)$.

The numerical integration limits are chosen in accordance with

$$(\delta\omega/\omega)^{(i)}_{\mathrm{PXR}} - c\operatorname{Im}\chi_0 < \delta\omega/\omega < (\delta\omega/\omega)^{(i)}_{\mathrm{PXR}} + c\operatorname{Im}\chi_0$$

where $(\delta\omega/\omega)^{(i)}_{\mathrm{PXR}}$ is the ith peak coordinate; $c \simeq 10^1$–10^2 is the input data parameter. The intervals are reduced in the case of crossing limits from neighbouring peaks.

Thus, in this section the method of computing PXR angular distributions in the case of multiple-diffraction PXR production was developed. This makes the simulation of experiments possible in principle. However, the time for the computation is very long: $\simeq 10$ values per minute for a PC 486 (50 MHz) when computing the three-wave generation, while the experiment simulation requires a distribution $\simeq 100 \times 100$ to be computed and the performance drops as the third power of the diffraction order. So, computation rate enhancement is a very significant problem.

† Complex roots will be complex conjugated in pairs because the equation has real coefficients.

5. Methods to increase the computation rate

Because of the publication space limits let us consider only the main notions on the time reduction of the PXR angular distribution computation, without details of their realization.

5.1. Rejection of weak peaks

There are $2N-2$ PXR peaks for each angular point $(\theta_1,\ \theta_2)$. However, the only intense peaks are those for which the parametric resonance condition coincides with the diffraction maximum, i.e. the peaks for which $|\ \alpha_h\ | \leqslant 1$. The computation time could be reduced by several times if we analyse the maxima of the PXR spectral-angular density in the centres of peaks and reject the weak peaks.

5.2. Reduction of the dimension of the diffraction matrix

Let us assume that an intense peak of the PXR spectral-angular distribution has been found. It is reasonable to analyse the value of reflex parameters α_m and exclude lines and columns corresponding to reflexes with $|\ \alpha_m\ | \gg |\ \chi_m\ |$ in the diffraction matrix, i.e. to decrease the order of diffraction before integrating over $\delta\omega/\omega$ in the neighbourhood of this peak. This procedure ensures a further computation-time reduction by four to eight times since seeking the eigenvalues (7) and solving the boundary problem (10) are accelerated.

5.3. Analytic integration of the PXR peaks

The analytic integration procedure has been used earlier in [8] and [9] for the two-wave PXR production. The notion is based on the fact that the width of a PXR peak for frequency ($\simeq$ Im $|\ \chi_h\ |$) is 10^1–10^3 times less than the width of a Bragg peak ($\simeq|\ \chi_h\ |$). Therefore, the parameters $\lambda_p^{(j)}(\omega)$ and $D_h^{s(j)}(\omega)$ can be considered as constant within a peak and taken outside the integral sign in (30), and the change of $\epsilon^{(j)}(\omega)$ can be allowed for in linear approximation. After that the integral (30) is easily calculated analytically if the derivative $d\epsilon^{(j)}/d\omega$ in the centre of the peak is known.

For the multiwave case the analytic integration is also possible but complicated by the three following circumstances.

(1) Several peaks exist and the contributions of intersection domains into the total integral should be accounted for. In particular, the structure of the scattering matrix (8) shows that if $|\ \alpha_h\ | > |\ \chi_h\ |$, then the roots ϵ^σ and ϵ^π are close ($\epsilon \simeq \alpha_h$) and, therefore, the peaks of σ and π polarizations are always close.

(2) The derivative $d\epsilon^{(j)}/d\omega$ can only be computed numerically, and since every point has $2N$ roots (the function $\epsilon^{(j)}(\omega)$ is many valued), careful precautions should be taken in order to ensure that the roots are not confused at the computation of the derivative.

(3) A multiwave Borrmann effect may appear in a narrow domain comparable with $\delta\omega/\omega \simeq$ Im $|\ \chi_h\ |$. In this case the solutions of the diffraction problem change in the same $\delta\omega/\omega$ scale as the PXR peak. To exclude errors in this domain, one should refrain from analytical integration if several parameters α_m simultaneously satisfy the condition $|\ \alpha_m\ | < |\ \chi_m\ |$.

Our experience shows that analytic integration is possible in 30–90% of cases and that it provides an advantage in the computation rate by 2–10 times.

On the whole, the use of the described and some other methods allows us to reduce the duration of computation by 30–40 times.

6. Computation of the PXR generation into the forbidden reflex simulated by three-wave diffraction

The algorithm developed has been used for simulation of the PXR generation with wavelength $\lambda = 1.54$ Å into the forbidden reflex (222) in the Ge crystal ($\chi_{222} = 0$). The reflex (222) is indirectly excited (simulated) by the three-wave Bragg diffraction on the planes $(3\bar{1}\bar{1})$ and $(\bar{1}33)$ (the Renninger effect). The computation parameters are as follows: the crystal surface coincides with the plane $(01\bar{1})$; the crystal plate thickness $L = 250$ μm; the electron with the energy $E = 1.2$ GeV is incident on the surface at an angle of 52.9°; the radiation length of the electron multiple scattering is $L_R = 15 \times 10^4$ μm. As all the diffraction planes are perpendicular to the surface, the symmetrical Laue case of diffraction occurs.

The intensity of radiation into the forbidden reflex is high only in the multiwave domain. Therefore, the multiwave effects are most pronounced in this case.

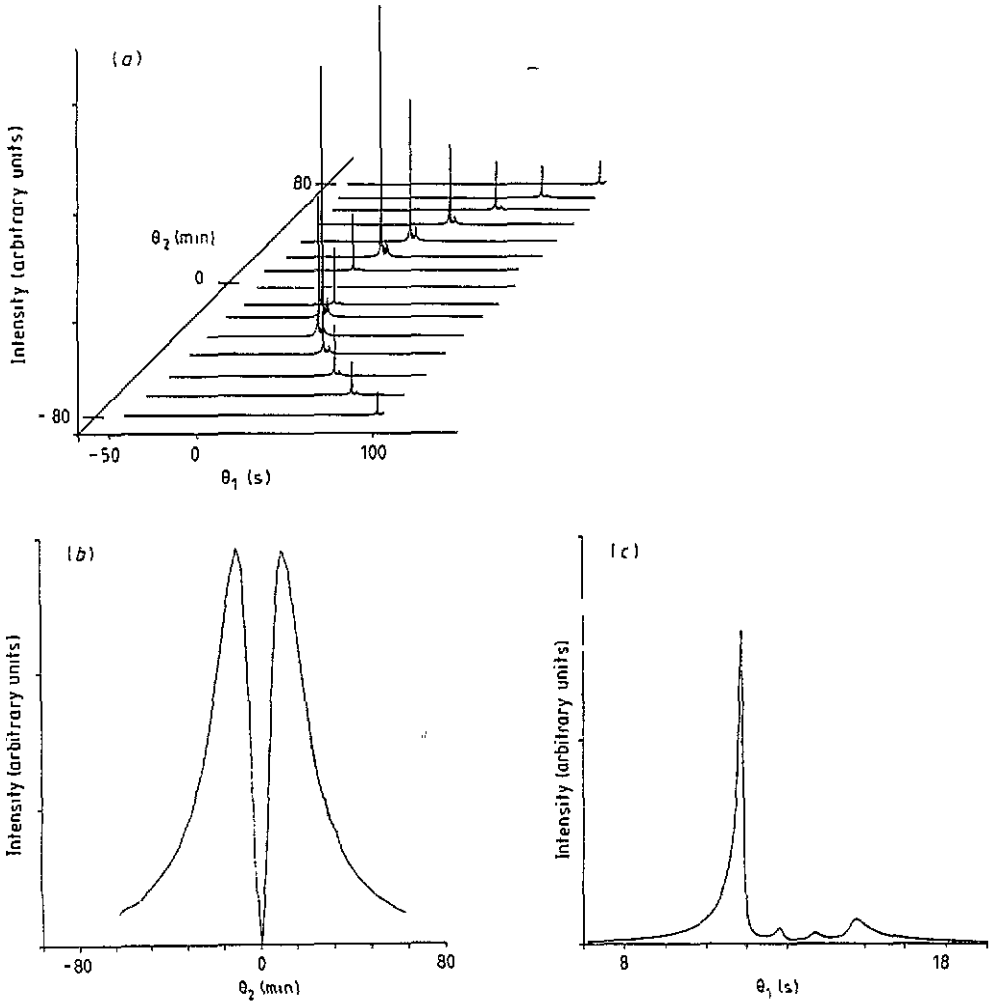

Figure 3. Two-dimensional angular distribution of three-wave PXR in the case of the simulated forbidden Bragg reflex in Ge (*a*), projection of this distribution into the reference plane θ_2 (*b*) and the section along θ_1 with $\theta_2 = 10'$ (*c*).

The general view of the PXR angular distribution is given in figure 3(*a*). The angular distribution has the form of a slightly curved 'prolongated touch' with divergence parameters $\simeq 5 \times 5000$ angular s. This distribution has a qualitative difference from the two-wave distribution, which is rather wide in both directions.

Let us make a more detailed comparison (see, e.g., [8]). Figures 3(*b*) and (*c*) show the projection of the angular distribution into the reference plane θ_2 and the section along θ_1 with $\theta_2 = 10'$. If the projection in figure 3(*b*) is qualitatively similar to the two-wave case, the section in figure 3(*c*) shows the basic difference: its width is $\simeq 10^3$ times less than that along θ_2, while the width of two-wave PXR peaks is of the same order in both directions. The difference of the angular distribution divergence relative to the angles θ_1 and θ_2 is attributed to the fact that the angle θ_1 is varied in the surface plane and θ_2 in the plane normal to the surface. Therefore, scanning in θ_1 causes the changes in all α_m, while the contribution of the θ_2 variations to α_m could be compensated by the change in $\delta\omega/\omega$.

Figure 3(*c*) clearly shows the fine structure of the PXR angular distribution. There are four peaks ($2N - 2$ in a general case); however, one of them is considerably more intense than the others. The half-width of this peak is less than 5 angular s.

It is essential that the spectral-angular distribution has a divergence $\simeq 5 \times 5$ angular s, i.e. it is collimated in the two planes. Thus, the considered three-wave PXR, concerning its spectral and angular characteristics, is similar to x-ray tube radiation collimated by two mutually perpendicular monochromator crystals. Hence, the multiwave PXR could be used as a source for investigations of x-ray multiple diffraction, small-angle scattering, etc. The wavelength of this source could be easily tuned by changing the angle of electron incidence on the crystal surface.

7. Conclusions

The algorithm and the program for the computation of the PXR spectral-angular and angular distributions produced by ultrarelativistic particles in crystals under multiple Bragg diffraction have been developed.

It is shown that using the multiple PXR generation it is possible to generate x-ray beams with double angular collimation $\simeq 1$ angular s^2 and spectral width $\delta\omega/\omega \simeq 10^{-3}$.

Acknowledgments

The authors are grateful to Professors V G Baryshevsky, I D Feranchuk, V G Kohn and G Ya Slepian for very useful discussions.

References

[1] Baryshevsky V G and Feranchuk I D 1971 *Zh. Eksp. Teor. Fiz.* **61** 944; correction: 1973 *Zh. Eksp. Teor. Fiz.* **64** 760
[2] Adyschev Yu N, Baryshevsky V G, Vorob'ev S A *et al* 1985 *Pis. Zh. Eksp. Teor. Fiz.* **41** 295
[3] Baryshevsky V G, Danilov V A, Ermakovich O L *et al* 1985 *Phys. Lett.* **110A** 477
[4] Baryshevsky V G and Feranchuk I D 1983 *J. Physique* **44** 913
[5] Baryshevsky V G and Feranchuk I D 1984 *Phys. Lett.* **102A** 141
[6] Afanasenko V P, Baryshevsky V G, Gradovsky O T *et al* 1989 *Phys. Lett.* **141A** 311
[7] Afanasenko V P, Baryshevsky V G, Gatsikha S V *et al* 1990 *Pis. Zh. Eksp. Teor. Fiz.* **51** 213
[8] Baryshevsky V G, Grubich A O, Feranchuk I D and Ivashin A V 1986 *Nucl. Instrum. Methods* A **249** 306

[9] Baryshevsky V G, Grubich A O and Feranchuk I D 1986 *Zh. Eksp. Teor. Fiz.* **90** 1588
[10] Truong Ba Ha and Dubovskaya I Ya 1989 *Phys. Status Solidi* b **155** 685
[11] Dubovskaya I Ya, Truong Ba Ha and Le Tien Hai 1991 *Phys. Status Solidi* b **165** 571
[12] Kohn V G 1979 *Phys. Status Solidi* a **54** 375
[13] Pinsker Z G 1981 *Dynamical Scattering of X-Rays in Crystals* (Berlin: Springer)
[14] Lugovskaya O M and Stepanov S A 1991 *Kristallografiya (USSR)* **36** 856
[15] 1980 *NAG Fortran Library Manual* Mark 8 (Oxford: NAG)
[16] Moler C B and Stewart G W 1973 *SIAM J. Numer. Anal.* **10** 241
[17] Andriyanchik A A, Dubovskaya I Ya and Kaminsky A N 1991 *J. Phys. C: Solid State Phys.* **3** 5579